ChemComm

COMMUNICATION

View Article Online
View Journal | View Issue

Cite this: *Chem. Commun.*, 2021, **57**, 2563

Received 30th November 2020,
Accepted 1st February 2021

DOI: 10.1039/d0cc07808e

rsc.li/chemcomm

A tumor microenvironment (TME)-responsive nanoplatform for systemic saporin delivery and effective breast cancer therapy†

Qian Shen,‡[a] Lei Xu,‡[b] Rong Li,*[a] Guang Wu,[a] Senlin Li,[b] Phei Er Saw,[b] Yusheng Zhou*[ac] and Xiaoding Xu *[ab]

Intracellular delivery of therapeutic proteins remains a challenge for the success of protein-mediated disease treatment. We herein develop a robust nanoplatform made with a TME-pH responsive Meo-PEG-*b*-PPMEMA polymer and a cationic lipid-like compound G0–C14 for *in vivo* delivery of cytotoxic saporin and breast cancer therapy. This nanoplatform could respond to a TME pH to rapidly release saporin/G0–C14 complexes, which could significantly improve the uptake of cytosolic saporin by tumor cells and subsequent endosomal escape, thereby leading to an effective inhibition of tumor growth.

Proteins play vital roles in various cellular processes (*e.g.*, signaling transduction, metabolism, and gene regulation) and their dysfunction is widely involved in the development and progression of various diseases, including cancer.[1–3] Therefore, protein therapy has shown great potential for cancer therapy with the advantages of high selectivity, strong activity, and low toxicity.[4] However, due to their intrinsically vulnerable structure and susceptibility to enzymatic degradation, most therapeutic proteins (*e.g.*, enzymes, growth factors, and cytokines) suffer from poor physicochemical/biological stability and potential immunogenicity.[5,6] In addition, when therapeutic proteins function in the cytoplasm, their internalization and biological activity are significantly restricted by poor membrane permeability and weak endosomal escape ability. Therefore, the development of an effective protein delivery strategy is essential to improve therapeutic outcomes.

In the past few decades, nanoparticles (NPs) have emerged as an important tool for systemic drug delivery.[7] Due to their advantages such as long blood circulation and high tumor accumulation, various NPs made with cationic lipids, polymers, or lipid/polymer hybrids have been developed for spatially and temporally controlled protein delivery.[8–12] Nevertheless, the *in vivo* therapeutic efficacy of proteins is still unsatisfactory due to their weak uptake and/or slow release in the target cells. Arising from the distinguishing tumor microenvironment (TME) compared to normal tissues, TME-responsive NPs have been recently designed and developed for effective cancer therapy. These NPs can respond to a TME signal (*e.g.*, acidic pH and hypoxia)[2] to change their physicochemical properties such as size, surface charge, and hydrophilic–hydrophobic balance, thereby inducing enhanced diffusion, cellular uptake, and/or intracellular cargo release.[13–16] At present, TME-responsive NPs have been successfully applied for the systemic delivery of chemotherapeutic drugs to achieve a better anticancer effect. Nevertheless, few efforts have been made to develop TME-responsive NPs for *in vivo* delivery of therapeutic proteins. We have previously reported a polymeric NP platform made with TME pH-responsive PEGylated polymer, and demonstrated its feasibility to improve *in vivo* small interference RNA (siRNA) delivery efficacy.[17] Since both siRNA and protein are biomacromolecules, this TME pH-responsive polymer may be also applicable for systemic protein delivery. However, the anticancer mechanisms of siRNA and therapeutic protein are totally different, *i.e.*, siRNA silences protumoral gene expression but therapeutic protein directly induces cell death; therefore, a technology platform still needs to be rationally designed to achieve efficient protein delivery *in vivo* and effective cancer therapy.

To achieve this goal, we herein report a robust NP platform, which is composed of our previously reported TME-responsive PEGylated polymer[17] and an amphiphilic cationic lipid-like compound (alkyl-modified polyamidoamine dendrimer, denoted as **G0–C14**),[18] for systemic protein delivery and effective cancer therapy (Fig. 1). After encapsulation of the therapeutic protein,

[a] *Institute of Pharmacy & Pharmacology and the Second Affiliated Hospital, University of South China, Hengyang 421001, P. R. China. E-mail: l7979r@163.com, yszhou08@126.com*
[b] *Guangdong Provincial Key Laboratory of Malignant Tumor Epigenetics and Gene Regulation, Medical Research Center, Sun Yat-sen Memorial Hospital, Sun Yat-sen University, Guangzhou 510120, P. R. China*
[c] *The Affiliated Nanhua Hospital, University of South China, Hengyang 421001, P. R. China. E-mail: xuxiaod5@mail.sysu.edu.cn*

† Electronic supplementary information (ESI) available. See DOI: 10.1039/d0cc07808e

‡ These authors contributed equally to this work.

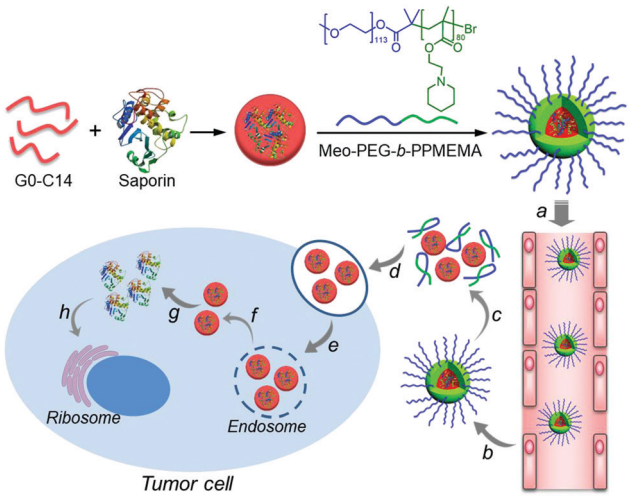

Fig. 1 Schematic illustration of the TME pH-responsive NP platform for systemic saporin delivery and breast cancer therapy. After encapsulation of saporin and then intravenous administration (a), the NPs could extravasate from the leaky tumor vasculature and accumulate in the tumor tissues (b). In response to TME pH, the NPs rapidly disassemble to release saporin/**G0–C14** complexes (c), which could be internalized by tumor cells (e) and then escape from endosomes to cytoplasm (f). With the cytosolic release of saporin (*g*), tumor growth is inhibited *via* saporin-mediated blocking of the protein synthesis function of ribosome (*h*).

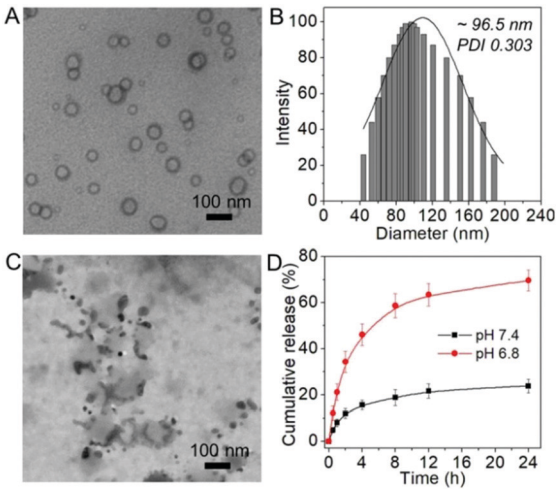

Fig. 2 (A and B) Morphology (A) and size distribution (B) of the NP50 platform in aqueous solution at pH 7.4. (C) Morphology of the NP50 platform in aqueous solution at pH 6.8. (D) Cumulative saporin release from the NP50 platform in aqueous solution at pH 7.4 or 6.8.

the resulting NP platform shows the following features for cytosolic protein delivery: (i) the hydrophilic PEG outer shell prolongs blood circulation[19] and thereby enhances tumor accumulation *via* the enhanced permeability and retention (EPR) effect;[20] (ii) TME pH-triggered protonation of the hydrophobic poly(2-(pentamethyleneimino)ethyl methacrylate) (PPMEMA) segment leads to the rapid NP dissociation and exposure of protein/**G0–C14** complexes that could enhance protein uptake; (iii) the cationic characteristic of **G0–C14** could induce endosomal swelling through the "proton sponge" effect[21] and thus improve endosomal escape of the internalized protein; and (iv) facile synthesis of the PEGylated polymer and robust NP formulation enables the scale-up of this NP platform. In this work, we chose the cytotoxic protein saporin and systematically evaluated the TME-pH responsive NPs for saporin delivery and its anticancer efficacy. Saporin is a type I ribosome-inactivating protein (RIP) that blocks the protein synthesis function of ribosome and induces apoptosis.[22] Due to the lack of a receptor, it is difficult for saporin to enter cells to implement its biological function. Our results show that systemic saporin delivery with the TME pH-responsive NPs could efficiently improve saporin uptake by tumor cells and significantly inhibit tumor growth.

The amphiphilic polymer, methoxyl-poly(ethylene glycol)-*b*-poly(2-(pentamethyleneimino)ethyl methacrylate) (Meo-PEG-*b*-PPMEMA), was synthesized *via* atom-transfer radical polymerization (ATRP) (Fig. S1 and S2, ESI†).[17] The pK_a value of this polymer was determined to be ~6.9 (Fig. S3, ESI†), which is close to the pH of tumor extracellular fluid (6.5–6.8),[23] suggesting that a TME pH-responsive protein release could be achieved when using a carrier made with this polymer. To verify our hypothesis, the classic nanoprecipitation method was used to prepare the NPs.[24] As shown in Fig. 2A, when mixing aqueous saporin solution with a dimethylformamide (DMF) solution containing Meo-PEG-*b*-PPMEMA and **G0–C14** followed by adding to rapidly stirred deionized water, well-defined NPs with a spherical morphology can be formed. In this self-assembly system, the negatively charged saporin could form complexes with the cationic lipid-like **G0–C14** in the DMF solution *via* electrostatic interaction with the hydrophobic tails of **G0–C14** positioned on the surface of the complexes.[11] When adding these complexes to deionized water, they could be encapsulated into the hydrophobic cores of the self-assembled Meo-PEG-*b*-PPMEMA polymer *via* hydrophobic interaction with the PPMEMA segment.[17] We varied the feed composition to adjust the physicochemical properties of the saporin-loaded NPs. As the amount of **G0–C14** increases, the resulting NPs (denoted as NP30, NP50, NP75, and NP100) show increased saporin encapsulation efficiency from ~30.7% to 87.6% and particle size from ~80 to 150 nm (Fig. S4, ESI†). One possible reason is that increasing **G0–C14** amount induces stronger electrostatic interaction with saporin, leading to the encapsulation of more saporin into the NPs with larger size.

Having successfully constructed the saporin-loaded NPs, we next examined their TME pH response using NP50 platform as an example. As shown in Fig. 2C, when incubating the NPs in aqueous solution at pH 6.8, the spherical NPs (Fig. 2A) transform into large amorphous aggregates and small size particles, which may possibly correspond to the ionized polymer and exposed saporin/**G0–C14** complexes.[25] This morphological change is mainly due to the NP dissociation induced by rapid protonation of the Meo-PEG-*b*-PPMEMA polymer at a pH below its pK_a (*e.g.*, pH 6.8). The TME pH-triggered rapid NP dissociation is further proven by dynamic light scattering (DLS) analysis (Fig. S5, ESI†), in which particles ranging from several nanometers to thousand nanometers could be detected after incubating the NP50 platform in aqueous solution at pH 6.8 for several minutes. With this rapid NP dissociation, the NP50

platform shows a fast protein release at a TME pH. As shown in Fig. 2D, more than 60% of the loaded saporin has been released within 8 h at pH 6.8. In comparison, less than 20% of the loaded saporin is released at pH 7.4.

After validating the TME pH response, we next investigated whether this TME pH-triggered NP dissociation could enhance saporin uptake and improve its anticancer effect. Human breast cancer cells (MDA-MB-231) were incubated with the NP50 platform and the saporin uptake was viewed using a confocal laser-scanning microscope (CLSM). As shown in Fig. 3A, the bright red fluorescence demonstrates that the NP50 platform could indeed improve saporin uptake compared to free saporin (Fig. S6, ESI†). More importantly, with the TME pH-triggered NP dissociation to expose saporin/**G0–C14** complexes, MDA-MB-231 cells show a higher saporin uptake at pH 6.8 than at pH 7.4. The similar tendency could be also found in the flow cytometry analysis (Fig. S7, ESI†), in which the saporin uptake at pH 6.8 is more than 3-fold higher compared to that of the cells treated with the NP50 platform at pH 7.4 (Fig. 3B). It is noteworthy that these internalized saporin molecules are mainly distributed in the cytoplasm (Fig. S8, ESI†), indicating that encapsulation of saporin into the TME pH-responsive NPs could enhance its endosomal escape *via* the "proton sponge" effect.[21] With the improved saporin uptake and efficient endosomal escape, the NP50 platform shows a stronger ability to induce apoptosis compared to free saporin. As shown in Fig. 3C and D, for the cells treated with the saporin-loaded NPs at pH 7.4, the percentage of apoptotic cells reaches around 34.5%, which is more than 3-fold higher compared to the cells treated with free saporin. Moreover, because the TME pH-triggered NP dissociation could significantly improve saporin uptake (Fig. 3A and B), the saporin-mediated apoptosis (~46.6%) is further enhanced at pH 6.8 (Fig. 3D). With this improved apoptosis, the cell death rate reaches ~50% (IC_{50} = 12.8 nM) after 24 h treatment with the saporin-loaded NPs at a saporin concentration of 10 nM (Fig. 3E). However, more than 70% of the cells are still alive after 24 h treatment with the NP50 platform at pH 7.4 (IC_{50} = 36.3 nM). In comparison, there is no obvious difference in the cell viability after 24 h treatment at pH 7.4 or 6.8 with the saporin-loaded NPs made with the methoxyl-poly(ethylene glycol)-*b*-poly(lactic acid-*co*-glycolic acid) (MeO-PEG-*b*-PLGA) (denoted as PLGA NPs), demonstrating the importance of the TME pH response to improve the cytotoxicity of saporin. Herein, *via* consideration of the particle size, zeta potential, saporin encapsulation efficiency, and IC_{50} value, the NP50 platform was selected for the next pharmacokinetics (PK) and biodistribution (BioD) experiments due to its relatively small size, moderate zeta potential, high encapsulation efficiency, and low IC_{50} value (Fig. S9, ESI†).

The PK study was conducted *via* intravenous injection of the saporin-loaded NPs into healthy mice (0.5 mg kg^{-1} saporin dose, n = 3). Compared to free saporin that is rapidly cleared from the blood (Fig. 4A) due to the protection of the PEG outer layer,[19] the NP50 platform shows long blood circulation with a half-life ($t_{1/2}$) of around 1.94 h. The BioD study was examined by intravenous injection of the saporin-loaded NPs into MDA-MB-231 xenograft tumor-bearing mice (0.5 mg kg^{-1} saporin dose, n = 3). As shown in Fig. 4B, the NP50 platform shows much higher accumulation in the tumor tissues compared to free saporin. This is mainly attributed to the long-circulating characteristic of the NP50 platform to improve its tumor accumulation *via* the EPR effect.[20] The major organs and tumor tissues were harvested at 24 h post-injection (Fig. S10, ESI†), and the NP distribution is shown in Fig. 4C. Free saporin mainly accumulates in the liver and kidney but not tumor tissues. In comparison, the saporin-loaded NPs show more than 5-fold higher tumor accumulation compared to free saporin.

We finally evaluated the *in vivo* anticancer effect of the NP50 platform *via* intravenous injection of the saporin-loaded NPs into MDA-MB-231 tumor-bearing nude mice (once every two days at a 0.5 mg kg^{-1} saporin dose, n = 5). After three consecutive injections, due to its high accumulation in the tumor tissues (Fig. 4B), the NP50 platform shows a much stronger tumor inhibition effect compared to other formulations (Fig. 4D–F). After 16 days post-treatment, there is around 2-fold increase in tumor size (Fig. 4D), which is lower than the tumor size increase of the mice treated by free saporin (4.1-fold), saporin-loaded PLGA NPs (3.1-fold), or the TME pH-responsive NPs without loading of saporin (control NPs, 7.3-fold). The similar tendency could be also found in the histological analysis of tumor tissues (Fig. 4G), in which the NP50 platform is the most effective in reducing cell proliferation. Notably, the administration of the NP50 platform shows

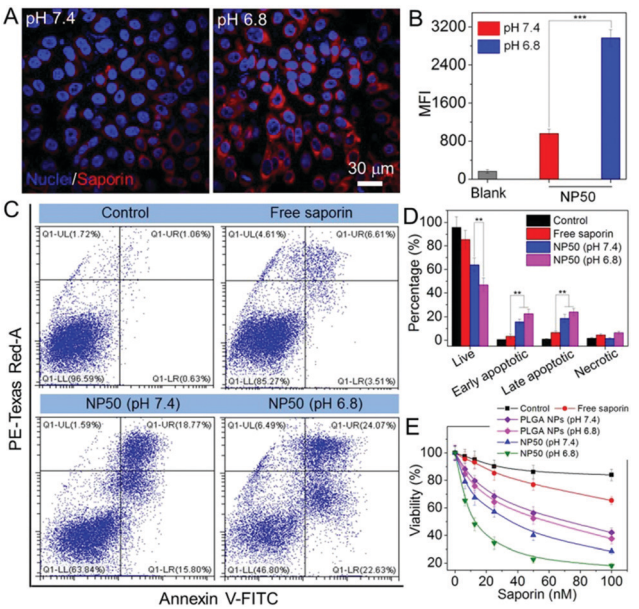

Fig. 3 (A and B) CLSM images (A) and mean fluorescence intensity (MFI, B) determined by flow cytometry analysis of MDA-MB-231 cells treated with the NP50 platform at pH 7.4 or 6.8 for 4 h. (C and D) Flow cytometry analysis (C) and quantification of apoptosis (D) of MDA-MB-231 cells treated with free saporin or NP50 platform at a saporin concentration of 10 nM for 24 h. $^{**}P < 0.01$; $^{***}P < 0.001$. (E) Viability of MDA-MB-231 cells treated with free saporin, NP50 platform or the saporin-loaded PLGA NPs for 24 h. The TME pH-responsive NPs without loading of saporin were used as a control.

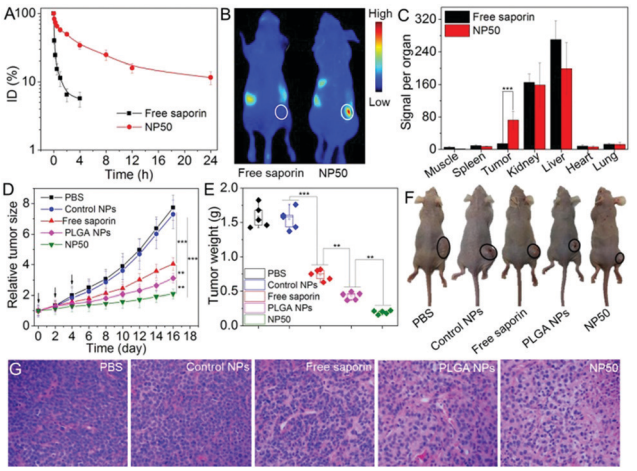

Fig. 4 (A) Blood circulation profile of free saporin and the NP50 platform. (B) Overlaid fluorescence image of MDA-MB-231 xenograft tumor-bearing mice at 24 h post-injection of free saporin or the NP50 platform. Tumors are indicated by ellipses. (C) Biodistribution of free saporin and the NP50 platform in the tumors and major organs of MDA-MB-231 xenograft tumor-bearing mice sacrificed at 24 h post-injection. (D and E) Tumor size (D) and weight (E) of MDA-MB-231 xenograft tumor-bearing mice treated with PBS, free saporin, NP50 platform, saporin-loaded PLGA NPs, and the TME pH-responsive NPs without loading of saporin (Control NPs). The intravenous injections are indicated by the arrows. $^{**}P < 0.01$; $^{***}P < 0.001$. (F) Representative photograph of MDA-MB-231 xenograft tumor-bearing mice in each group at day 16. Tumors are indicated by ellipses. (G) H&E staining of MDA-MB-231 tumor tissues after systemic treatment in each group.

negligible toxicity, as demonstrated by no influence on mouse body weight (Fig. S11, ESI†) and no noticeable histological changes in the tissues of heart, liver, spleen, lungs, and kidneys (Fig. S12, ESI†). This good biocompatibility is further confirmed by blood serum analysis, in which TNF-α, IFN-γ, IL-6, and IL-12 levels are within the normal range at 24 h post-injection (Fig. S13, ESI†).

In conclusion, we have developed a new TME pH-responsive NP platform for systemic saporin delivery and effective cancer therapy. This NP platform could highly accumulate in the tumor tissues and then rapidly respond to TME pH to expose the saporin/**G0–C14** complexes, which subsequently transport saporin into the cytoplasm to achieve efficient inhibition of tumor growth. The TME pH-responsive NP platform developed herein could be used as an effective vehicle for the systemic delivery of various cytotoxic proteins (*e.g.*, cytochrome *C* and apoptin) and cancer therapy.

This work was supported by the International Scientific and Technological Cooperation Program from Guangdong Science and Technology Department (2018A050506033) and the grant from Guangzhou Science and Technology Bureau (201902020015). The animal experiments were conducted in accordance with the Guide for the Care and Use of Laboratory Animals issued by the Ministry of Science and Technology of China and approved by the Institutional Animal Care and Use Committee at Sun Yat-sen University.

Conflicts of interest

There are no conflicts to declare.

Notes and references

1 F. Chiti and C. M. Dobson, *Annu. Rev. Biochem.*, 2017, **86**, 27–68.
2 D. Hanahan and R. A. Weinberg, *Cell*, 2011, **144**, 646–674.
3 C. A. Ross and M. A. Poirier, *Nat. Med.*, 2004, **10**, 10–17.
4 B. Leader, Q. J. Baca and D. E. Golan, *Nat. Rev. Drug Discovery*, 2008, **7**, 21–39.
5 D. S. D'Astolfo, R. J. Pagliero, A. Pras, W. R. Karthaus, H. Clevers, V. Prasad, R. J. Lebbink, H. Rehmann and N. Geijsen, *Cell*, 2015, **161**, 674–690.
6 S. Mitragotri, P. A. Burke and R. Langer, *Nat. Rev. Drug Discovery*, 2014, **13**, 655–672.
7 J. Shi, P. W. Kantoff, R. Wooster and O. C. Farokhzad, *Nat. Rev. Cancer*, 2017, **17**, 20–37.
8 M. Yu, J. Wu, J. Shi and O. C. Farokhzad, *J. Controlled Release*, 2016, **240**, 24–37.
9 M. Amidi, E. Mastrobattista, W. Jiskoot and W. E. Hennink, *Adv. Drug Delivery Rev.*, 2010, **62**, 59–82.
10 R. Mo, T. Jiang, J. Di, W. Tai and Z. Gu, *Chem. Soc. Rev.*, 2014, **43**, 3595–3629.
11 M. Wang, K. Alberti, S. Sun, C. L. Arellano and Q. Xu, *Angew. Chem., Int. Ed.*, 2014, **53**, 2893–2898.
12 S. Reinhard, H. Han, J. Tuma, J. J. Røise, I. C. Li, J. Li, H. Y. Lee and N. Murthy, *Chem. Commun.*, 2020, **56**, 14207–14210.
13 Y. Lu, A. A. Aimetti, R. Langer and Z. Gu, *Nat. Rev. Mater.*, 2016, **2**, 16075.
14 B. Chen, W. Dai, B. He, H. Zhang, X. Wang, Y. Wang and Q. Zhang, *Theranostics*, 2017, **7**, 538–558.
15 H. Xu, Y. Wang, Z. Pei, W. Ji and Y. Pei, *Chem. Commun.*, 2019, **55**, 14930–14933.
16 C. Lin, Y. Tao, P. E. Saw, M. Cao, H. Huang and X. Xu, *Chem. Commun.*, 2019, **55**, 13987–13990.
17 P. E. Saw, H. Yao, C. Lin, W. Tao, O. C. Farokhzad and X. Xu, *Nano Lett.*, 2019, **19**, 5967–5974.
18 Z. Bi, Q. Li, X. Dinglin, Y. Xu, K. You, H. Hong, Q. Hu, W. Zhang, C. Li, Y. Tan, N. Xie, W. Ren, C. Li, Y. Liu, H. Hu, X. Xu and H. Yao, *Adv. Sci.*, 2020, **7**, 2000915.
19 K. Knop, R. Hoogenboom, D. Fischer and U. S. Schubert, *Angew. Chem., Int. Ed.*, 2010, **49**, 6288–6308.
20 H. Maeda, *Adv. Drug Delivery Rev.*, 2015, **91**, 3–6.
21 W. He, X. Xing, X. Wang, D. Wu, W. Wu, J. Guo and S. Mitragotri, *Adv. Funct. Mater.*, 2020, **30**, 1910566.
22 I. Barthelemy, D. Martineau, M. Ong, R. Matsunami, N. Ling, L. Benatti, U. Cavallaro, M. Soria and D. A. Lappi, *J. Biol. Chem.*, 1993, **268**, 6541–6548.
23 Y. Wang, K. Zhou, G. Huang, C. Hensley, X. Huang, X. Ma, T. Zhao, B. D. Sumer, R. J. DeBerardinis and J. Gao, *Nat. Mater.*, 2014, **13**, 204–212.
24 L. Zhang, J. M. Chan, F. X. Gu, J.-W. Rhee, A. Z. Wang, A. F. Radovic-Moreno, F. Alexis, R. Langer and O. C. Farokhzad, *ACS Nano*, 2008, **2**, 1696–1702.
25 X. Xu, P. E. Saw, W. Tao, Y. Li, X. Ji, M. Yu, M. Mahmoudi, J. Rasmussen, D. Ayyash, Y. Zhou, O. C. Farokhzad and J. Shi, *Nano Lett.*, 2017, **17**, 4427–4435.

